Interannual-to-multidecadal climate variability and its relationship to global sea surface temperatures

David B. Enfield [1] and Alberto M. Mestas-Nuñez [2]

[1] NOAA Atlantic Oceanographic and Meteorological Laboratory

4301 Rickenbacker Cswy, Miami, FL 33149 USA

[2] Cooperative Institute for Marine and Atmospheric Studies

4600 Rickenbacker Cswy, Miami, FL 33149 USA

Resubmitted as a chapter in:

Present and Past Inter-Hemispheric Climate Linkages
in the Americas and their Societal Effects

V. Markgraf, (ed.), Cambridge University Press

February 1999

Abstract

As a benchmark to help profile paleoclimates across the Americas we develop an overview of what is known of modern climate variability on a planetary scale, with emphasis on climate manifestations in the Western Hemisphere. From instrumental observations taken as early as the mid-19th century, we look at both atmospheric and oceanic variables and consider their relationships on timescales ranging from interannual to multidecadal. We focus on three of the most important climate modes: the interannual El Niño-Southern Oscillation (ENSO), the interdecadal Pacific Decadal Oscillation (PDO) and the multi-decadal North Atlantic Oscillation (NAO). The variable of greatest interest is sea surface temperature (SST) because it is arguably the least understood of the atmospheric boundary conditions for prehistoric climates and yet one of the most critical for effecting atmospheric model simulations of those climates. The analysis begins by computing a global distribution of the trend in SST, which turns out to be highly non-uniform, with characteristics that may reflect low-frequency changes in shallow water mass formation. We then compute a global, canonical mode for ENSO that preserves the amplitude and phase structures of interannual ENSO variability worldwide. The ranking of the modal amplitudes of ENSO events differs from the absolute amplitudes obtained by indexing SST data directly. This reflects the importance of the (non-ENSO) decadal-multidecadal climate modes in modifying the intensity of ENSO-related ocean warmings. Comparing the global mode between the ends of the 19th and 20th centuries, we see essentially no difference in amplitudes and frequency of ENSO on the global warming timescale, although such changes have occurred on shorter, multidecadal timescales. Upon removal of the global ENSO mode from the data, the residual variability is subjected to two different analyses that extract very similar spatio-temporal patterns of SST for the PDO- and NAO-like climate modes. The climate variations with longer timescales (PDO, NAO) together account for about the same amount of variance as ENSO, globally, and in some regions, e.g., the northeastern North Pacific, may rival ENSO in their climate and marine impacts. The NAO, in particular, involves an Atlantic-Pacific connection that may arise through fluctuations in the polar vortex, an aspect which may also characterize previous climates. In our discussion, we speculate on what might be learned from the instrumental record regarding possible characteristics of ancient climates, especially regarding the possibility that ENSO may have been considerably different or even absent in the mid-Holocene.

Introduction

Progress in understanding pre-instrumental climate fluctuations requires a complex mix of climate-impact proxy analysis, modeling, past reconstruction of presently measured variables, and inferences from modern climate variability. The task that befalls this chapter (ocean emphasis), and the one by Dettinger et al. (Chapter XXX; atmospheric and continental emphasis), is to consider recent progress in understanding the instrumental climate record of the 19th and 20th centuries, how it may relate to previous climate variability, and how the paleoclimatic perspective may relate to future climate. The primary concern of this chapter is to consider the ocean's role in climate through the variability of sea surface temperature (SST). One purpose of the chapter is simply to bring paleoclimate investigators up to date on recent findings on the oceanographic and atmospheric aspects of modern climate. Another aim is to awaken the consciousness of the paleoclimate community to certain issues that must be considered for past climates in view of what we are learning about the present climate.

One of our hopes for projecting the present into the past is that we observe considerable self-similarity in the modern climate across timescales. This will therefore be commented upon as we describe the three principal timescales observed in more than a century of SST measurements: interannual (e.g., "El Niño"), decadal to multidecadal, and secular (global warming). However, as one delves into past climates more remote in time, and farther removed from the recent range of fluctuation, our confidence in projections based on self-similarity inevitably diminishes. Hence, we will put more effort into speculating on the Holocene (mainly 10 kyr BP to present) than on the pre-Holocene (more than 15 kyr BP). This is appropriate, of course, because the range of variations that occurred in the Holocene is more likely to be representative of what might be observed in the next century.

Data and methods

Except in the next section, we shall depend almost exclusively on the SST data that have been taken since the mid-19th century. However, a problem with using summary compilations of SST, such as the Comprehensive Ocean-Atmosphere Data Set (COADS, Woodruff et al., 1987), is that the sampling frequency and spatial coverage of ship observations has increased several-fold over the last 150 years. This has resulted in a record that is very inhomogeneous in both space and time. We therefore use a reanalyzed version of SST anomalies (SSTA) data by Kaplan et al. (1998, henceforth K98) wherein only the variability of large-scale patterns has been retained through a combination of multivariate filtering and inverse analysis. The K98 data are monthly on a 5°x5° global grid from 1856 through 1991. The K98 SSTA reanalysis is very similar to the one by which the contemporaneous relationship between tree-ring proxy data and modern, well-measured SST are used to reconstruct pre-instrumental SST variability (Chapter YYY by Evans et al.). With the K98 approach, confidence in the resolution of basin-scale features is increased at the expense of resolving small-scale features.

Although the methods used in the K98 reanalysis minimize the effects of poor sampling, we naturally have less confidence in the accuracy of the earlier maps relative to those after about 1950. If one examines decadal plots of ship tracks (Woodruff et al., 1987), it is clear that the historical ship sampling of SSTA is least complete in the southeastern South Pacific and in the southwestern South Atlantic. Although the tropical Pacific is more thinly sampled in the early part of the record, the important features are of large zonal scale (retained by the leading multivariate modes used in the K98 reanalysis) and their temporal fluctuations are probably resolved adequately by the mainly meridional ship tracks, east of the dateline, after about 1870 (Smith et al., 1998). The mid- and high-latitude regions of both the North Atlantic and North Pacific were comparatively well sampled through most of the reanalyzed period. All of the regions discussed in this chapter were fairly well sampled from 1890 onwards, and the Atlantic regions from the 1860s. We refer the reader to K98 for a more complete discussion of the reanalysis quality. In the SSTA analyses performed here we use the more reliable 1871-1991 period. We also refer frequently to similar calculations done by Enfield and Mestas-Nuñez (1999) and Mestas-Nuñez and Enfield (1999) for the entire (1856-1991) period of the K98 reanalysis.

Our first task (next section) will be to describe the secular trend in SSTA, globally, and the canonical global mode of SSTA associated with El Niño-Southern Oscillation (ENSO). Subsequent removal of these two components allows us to concentrate more confidently on the intermediate timescale (decadal-multidecadal) and on variability unrelated to interannual ENSO variations.

To establish a link between decadal-to-multidecadal SSTA variability and the associated atmospheric climate fluctuations, we consider how SSTA is related to commonly used atmospheric climate indices based on modern measurements of sea level pressure (SLP). These and similar indices have been used by many authors to characterize the temporal variability of land climate patterns. The analysis method used in this comparison is a simple composite of SSTA based on the positive and negative phases of the anomalous SLP (SLPA) indices. The SLP data used here are the 1899-1997 Northern Hemisphere (NH) monthly analyses available at the U.S. National Center for Atmospheric Research (NCAR), denoted DS010.0.

The third analysis is of the decadal to multidecadal SSTA variability using ordinary and rotated empirical orthogonal function (EOF) analysis after removing the linear trends and global ENSO mode. In that analysis we extract several global modes and compare them to the earlier SLPA-SSTA composites. In the final section, we shall discuss some of the implications of these analyses for previous climates.

Secular trends and the global ENSO mode

One reason for considering these two timescales first is that they will be removed from the data prior to analysis of decadal-multidecadal variability. It is also appropriate to discuss them together because of current speculation that global warming may affect ENSO variability (Trenberth and Hoar, 1996). More generally, the characteristics of ENSO, or even its existence (or lack of it) during prehistoric periods, may be dependent on the background climate (Sun, 1999). We shall redirect our attention to these timescales when we discuss the paleoclimate implications of modern measurements in a later section.

The global distribution of secular trends

Fig. 1 (top) is a map of the globally distributed linear trend in SSTA over a 136-year time period (1856-1991), based on a simple, unweighted linear regression of SSTA at each 5°x5° grid point on the monthly time vector. The associated temporal variation of the global mean SSTA (bottom) is relatively trendless prior to 1900 and has a more accentuated trend after that time. Therefore, while the trend map is representative of the true secular pattern after 1900, the magnitudes shown tend to underestimate the post-1900 trend by about 40%. We have tried alternate approaches for treating the secular change in the data, e.g., division into two periods with different means, and the description of the secular variation is not sensitive to the representation. We therefore adopted the simplest scheme (linear trend) rather than making necessarily arbitrary judgements.

At the largest, global scale, the overriding impression from the trend map is that warming trends dominate over cooling, and that the rate of secular change is highly inhomogeneous spatially. Off the equator, the shaded regions of largest positive trend (> 0.4°C per century) are in the South Atlantic, the subtropics of the central and eastern Pacific, the Gulf of Alaska and the region north of Cape Hatteras where the Gulf Stream separates from the eastern coastline of the continental United States. Regions of negative trend (< -0.2°C per century) are found in the mid-latitudes of the east-central North Pacific, and in the high-latitude region southeast of Greenland. The equatorial Pacific, of particular interest because of its importance for ENSO variations, shows only null or weakly positive trend between the Galapagos Islands and the dateline, strong cooling off Ecuador and Peru and warming west of the dateline. The equatorial Atlantic shows moderate warming that appears as a low-latitude extension of the stronger warming in the South Atlantic. Other than in the central South Pacific, all other regions are characterized by a mild warming trend of about 0.1-0.3°C per century.

The linear trends in the instrumental record shown here are the closest thing, in timescale, to the slow climate fluctuations that might be detected in previous epochs by less direct, paleoclimatic methods. Examples that come to mind are the Little Ice Age (LIA) and the Medieval Warm Period (MWP). To the extent that the latter imply globally warmer or cooler climates in the past, we must keep in mind that those patterns too may have been quite heterogeneous and that certain regions may also have been cooling (warming) when the Earth as a whole was warming (cooling). This lack of homogeneity is confirmed by the 500-year atmospheric model simulation of Hunt (1998), which reproduces ~100 year-long periods of globally warmer or cooler air temperatures similar to the LIA and MWP. Extreme decadal averages in these periods, which occur as natural (externally unforced) climate variability in the model, exhibit large contiguous areas of ocean and land with anomalies opposite to the contemporaneous global mean. This reinforces the likelihood that a period like the mid-Holocene would have had very non-uniform differences from our present climate. This could be especially significant if the ancient patterns of SST change were anything like Fig. 1, because the regions with trends counter to the global averages are in the North Pacific and North Atlantic where present-day water masses are formed and subducted (Nakamura et al., 1997; Curry et al., 1998). Those processes are currently suspected of playing an essential role in the shifts between climate regimes. The existence of such inhomogeneities at the secular timescale implies that similar feedbacks may play a role in climate variations with centennial or longer timescales, in the future as well as the past.

The linear trends were removed from the K98 data prior to the removal of the ENSO mode described in the next section. The order in which these removals were done has no effect on the residual (trendless, non-ENSO) variability. All discussions of the SSTA variance explained by the various components of variability have been referred to the detrended data set.

The global ENSO mode

The interannual ENSO signal gets distributed from the Pacific to other tropical oceans through its associated global tropospheric anomalies (Hastenrath et al., 1987; Latif and Barnett, 1995; Lanzante, 1996; Enfield and Mayer, 1997; Enfield and Mestas-Nuñez, 1999). The characteristic lag of the extended ENSO response in the Atlantic and Indian Oceans is approximately one to three seasons, which is comparable to the lag of the high latitude North Pacific with respect to the tropical Pacific. This is not a mere curiosity. According to Lau and Nath (1994), if the extended ENSO signal in other ocean basins is not included in a global coupled model, the model cannot accurately replicate the tropospheric response, such as the Pacific North American (PNA) pressure pattern (Barnston and Livezey, 1987). On the other hand, if one wishes to understand the relationship between land climate and another climate mode such as the North Atlantic Oscillation (NAO), the existence of the ENSO signal in the Atlantic makes unequivocal attribution difficult.

To better characterize the global ENSO mode of variability, we have performed a complex EOF analysis of the monthly K98 data that correctly preserves the phase lags within the Pacific and in other oceans. The detrended data are first bandpassed to block periodicities larger than eight years or shorter than 1.5 years. The leading mode of the decomposition is the one that represents the global ENSO. It explains 13.4% of the variability in the detrended, unfiltered data set for the December-January-February (DJF) season. For additional details on the methods used, the reader is referred to Enfield and Mestas-Nuñez (1999). However, we have repeated the Enfield and Mestas-Nuñez calculation here for the shorter but more reliable 1871-1991 period. The differences between the two analyses are small and the conclusions are essentially unchanged.

Because the ENSO mode is based on a complex decomposition of the data, it has complex eigenvectors and expansion coefficients, which can be transformed into amplitudes and phases in both the spatial and temporal domains. We show the spatial amplitude and phase in the top two panels of Fig. 2. The obvious reference rectangle to characterize the ENSO mode is the well-known NINO3 region in the equatorial Pacific, bounded by 5°N-5°S, 90°W-150°W (middle). The spatial amplitude (top) is shown as a percent gain with respect to the reconstructed temporal amplitudes for NINO3 (bottom). Thus, the average gain in the NINO3 rectangle is 100 and the contour labeled 30 passes through regions where the amplitude is 30% of the NINO3 amplitude. Significance tests on the correlation coefficients between the data and the temporal reconstruction show that amplitudes in the white regions (<10) are insignificant. For ease of display, the spatial phase (middle) has been transformed into a temporal lag at each grid point (units of three-month seasons), referenced to the NINO3 phase at a nominal mid-band periodicity of 43.7 months (determined from zero upcrossings in the temporal reconstruction).

To represent the temporal behavior of the mode (bottom) we show the temporal reconstruction (temperature units) for phases and amplitudes combined over an index region rather than the more confusing temporal amplitude and phase functions from which they are derived (i.e., the complex expansion coefficients for the mode). The modal time variability elsewhere is merely the same series lagged by the appropriate spatial phase and with amplitude attenuated in proportion to the spatial amplitude.

The gain and phase maps show the well-known features of mature El Niño events in the Pacific: maximum amplitude within ±10° of the equator, opposite phase in the mid-latitudes of the central North and South Pacific, and near-coastal lags increasing to 1-2 seasons poleward of the reference region. Amplitudes in the tropical Atlantic and Indian Oceans are 10-15% of the NINO3 amplitude, and the extrema occur 1-3 seasons after the maximum NINO3 amplitude. The delayed responses in the Atlantic and Indian Oceans have been noted by previous studies (e.g., Enfield and Mayer, 1997; Latif and Barnett, 1995).

The larger positive peaks in the temporal reconstruction correspond to historical El Niño events (e.g., Quinn et al., 1987). ENSO activity has varied over more than a century of measurements, as evidenced by the relatively quiescent decades following the 1941-42 event. However, there is no visually detectable difference between the first 30 years of the record (1875-1905) and the last 30 years (1960-1990); both periods had about 7-9 events of similar intensities. Hence, there is no obvious indication, in this representation, that global warming has had a significant effect on the ENSO activity.

The global ENSO mode is a canonical representation of the spatial and temporal commonalities found in the ENSO extrema of the historical SSTA data. Filtering has removed the modifying effect that long-period anomalies have on ENSO amplitudes, as well as the frequently occurring double peaks and other temporal details caused by fluctuations of annual and shorter timescale. Nor are the unusual aspects of individual ENSO extrema captured; rather, they are relegated to higher modes. As a result, the amplitudes are generally smaller than an unfiltered data average over the NINO3 region.

Significantly, the reconstructed event amplitudes sort differently than for the data-averaged NINO3 index (not shown). Thus, 1983 has the fifth largest positive amplitude in the reconstructed series, rather than one of the two largest in the data, and 1972 is one of the two largest reconstructed events (along with 1878). The main reason for this change in rank is that 1972 occurred during a 2-3 decade period of generally lower background temperatures, whilst 1983 occurred after Pacific interdecadal variability at low latitudes had flipped from negative to positive background values in the late 1970s. Much of the 1983 amplitude is captured instead by the leading EOF modes of the non-ENSO residual data (later section).

Decadal-multidecadal climate fluctuations

In recent years there has been increased recognition that smaller (than ENSO) but significant climate shifts occur on timescales from decadal to multidecadal. Such fluctuations may be related to ocean-atmosphere interactions, amenable to simulation and prediction by numerical models. An example in the tropics is the interdecadal succession of comparative rainy periods with drought periods in the Sahel region of sub-Saharan northwest Africa (Nicholson, 1989), along with its strong association with the frequency of Atlantic tropical cyclones (Gray, 1990). Climate shifts have also been noted in rainfall and air temperature for the Northern Hemisphere extratropics, especially in central and northern Europe and in western North America. These slow climate oscillations correspond to upstream (to the west) fluctuations in the mid-latitude westerly wind belts and associated persistent features in atmospheric pressure patterns, such as the Aleutian Low, the Icelandic Low and the Azores High. Two dominant and quasi-independent oscillations have been noted: the Pacific Decadal Oscillation (PDO) and the North Atlantic Oscillation (NAO). The index time series frequently used to represent the tropospheric variability of the PDO and NAO are based on long records of sea level pressure (SLP) measured near, or interpolated to the critical nodal points of SLP anomaly (SLPA) patterns.

We are concerned to know what the non-ENSO patterns of variability in SSTA are and how they relate to these climate oscillations. Hence, in this section we will show SLPA-based index series for the PDO and NAO with their composite mean SLPA maps over the Northern Hemisphere, and then show the corresponding composite maps for SSTA. The composite SSTA maps can then be used as a reference for the non-ENSO global modes to be discussed in the next section.

For the Pacific PDO, the index we have chosen is the DJF average of SPLA over the Aleutian Low region, 167.5°W-177.5°W, 42.5°N-52.5°N. Trenberth and Hurrell (1994) and Latif and Barnett (1996) have used similar Pacific indices. In Fig. 3 (top) we show the PDO index time series and a smoothed version of it using a loess filter, which is a locally weighted quadratic smoother, with a half span of 8 years. Also shown (middle) is a polar-projected NH map of the difference between composite means of the winter SLPA data, based on positive and negative values of the index series. The bottom panel shows the K98 SSTA, similarly composited on the PDO index. The corresponding DJF plots for the Atlantic NAO are shown in Fig. 4, where for the NAO index we have chosen to use the difference of normalized SLPA between Lisbon, Portugal and Stykkisholmur, Iceland, previously used by Hurrell (1995). Both SLPA indices are signed to be positive when pressures at higher latitudes are negative and the mid-latitude westerlies south of the negative pressure node are anomalously strong.

The positive phase of the PDO is characterized by an enhanced Aleutian Low and strengthened westerly winds over the mid-latitude central North Pacific (Fig. 3, middle). There is also some weakening of the polar vortex but the pattern is neutral over the rest of the Northern Hemisphere. The smoothed index was positive from 1925-1945, negative during 1945-1975 and positive again after the mid-1970s (Fig. 3, top). The dominant timescale of the smoothed PDO is shorter (1-3 decades) than that of the NAO (> 25 years). The high (low) index state is associated with greater (less) winter storminess over the central North Pacific and a warmer (cooler) winter climate along the west coast of North America (Latif and Barnett, 1994; Wiles et al., 1998).

The SSTA imprint of the PDO's positive (negative) phase is dominated by an extensive zone of cooler (warmer) SST over the Kuroshio Extension region (40°N) east of Japan as far as 145°W (Fig. 3, bottom). This too is consistent with enhanced (diminished) evaporation and mixing under the stronger (weaker) westerly winds, and thus enhanced (diminished) cooling over that region. SSTA of opposite sign and equally as large in amplitude is found in the northeastern North Pacific, consistent with observed warmer land temperatures over western North America (Wiles et al., 1998). Accompanying an enhanced Aleutian Low (high PDO index), west coast warmings are consistent (in an advective sense) with an enhanced poleward ocean circulation in the subarctic gyre of the northeast Pacific and a diminished equatorward California Current System to the south. Corresponding to the North Pacific changes, there is also warming south of the equator in the eastern Pacific, extending poleward to the Chilean coast. Most attempts to explain the SSTA signature of the PDO invoke ocean-atmosphere interactions in the North Pacific, but no clear explanation has yet been proposed for the features off South America.

We note that the overall spatial pattern of SSTA for the PDO looks very much like the ENSO pattern, but with weaker and broader warming in the eastern tropical Pacific, and more intense cooling over the central North Pacific. As with the warm phase of ENSO, the warm eastern Pacific observed since the mid-1970s is associated with a migration of salmon stocks northward from Oregon-Washington to the Gulf of Alaska (Mantua, et al., 1997), and a replacement of anchovies by sardines and horse mackerel populations off Peru and Chile (Muck, 1989).

In the high index state of the NAO (Fig. 4, middle) the polar vortex is intensified with enhanced low pressures concentrated in the Greenland region, while pressures are high over the Azores. Westerly winds blow more strongly across the North Atlantic between the two nodes. The NAO has been in its high index state since about 1970, preceded by low values in the 1950s and 1960s (Fig. 4, top). A previous high state during the 1905-1930 period was followed by 25 years of near-normal values. Timescales range from less than a decade to multidecadal. Under extremes of the NAO, comparatively severe winters (high rainfall) alternately affect northern (high index) and southern (low index) Europe (Hurrell, 1995). The NAO and its climate impacts are consistent with inferences drawn from tree ring records around the North Atlantic basin (D'Arrigo et al., 1996). In the tropical sector, a high (low) index is associated with less (more) rainfall in the African Sahel (Nicholson, 1989) and less (more) tropical cyclone development west of NW Africa

(Gray, 1990). That the NAO may now be returning to the low-index phase is suggested by the recent rapid fall in the unfiltered data (Fig. 4, top) and confirmed by a multivariate mode in the updated global SSTA, similar to the Atlantic mode discussed in the next section (Landsea et al., 1999).

The winter (DJF) SSTA distribution corresponding to the high phase of the NAO (post-1970) shows moderately warmer conditions in the western mid-latitudes of the North Atlantic (35°N-40°N), roughly west of the intensified Azores High and sandwiched between enhanced westerlies to the north and easterlies to the south (Fig. 4, bottom). Cooler temperatures are found under the latter zones of enhanced wind speeds (40-50°N, 15-20°N). Although this cooling is consistent with greater evaporation rates at the short timescales, the modeling study of Timmerman et al. (1998) argues that the >35-year timescale is primarily controlled by changes in the thermohaline circulation (THC). At intermediate timescales advection may play a greater role and for the shorter timescales, diabatic heating due to surface fluxes and thermocline entrainment become increasingly important (e.g., Bjerknes, 1964; Halliwell, personal comm.). The tropical South Atlantic is neutral with respect to the NAO and the high latitude South Atlantic is moderately warm when the index is positive. One must be cautious in regard to the last feature, however, because sampling is relatively poor south of 30°S and west of the Greenwich meridian. When considered over all months (not shown), the warming region in the midlatitude North Atlantic is stronger and more zonally extensive, while the warming in the extratropical South Atlantic disappears.

The SSTA signature of the NAO includes an inter-ocean feature in the Pacific: when the NAO index is high (low) SSTAs along the US west coast, in the Gulf of Alaska, and in the central equatorial Pacific are significantly cooler (warmer). Again, the Pacific region resembles the ENSO pattern, but as we point out in the next section, these climate modes do not necessarily separate cleanly, and alternate representations with differing Pacific signatures may be equally, or more, reasonable.

Global modes of SSTA variability

After removal of the interannual global ENSO mode (Fig. 2) from the K98 SSTA data, we computed the ordinary (not complex) EOFs of the non-ENSO residuals for the DJF season, 1871-1991. The first three leading modes explain 6.1%, 5.4% and 3.6% of the residual unfiltered variance after removal of trends. The total – 15.1% -- is comparable to the 13.4% explained by the global ENSO mode for the same season. As frequently occurs when the geographic scale of a data set is much larger than the scales of the physical processes, the leading global EOFs include contributions from different ocean basins. Such regions may be physically linked through teleconnective processes, or they may associate statistically by accidentally conforming to a common principal axis of variation. We therefore applied a varimax rotation (REOF) to the first 10 EOF modes so as to separate regional processes that are more appropriately considered independently of each other. This was done so as to preserve spatial orthogonality between REOF modes while relaxing temporal orthogonality, meaning that zero-lag temporal correlations are allowed as the leading (unrotated) modes are reconfigured. The unrotated EOFs are very similar to those of Enfield and Mestas-Nuñez (1999), and the REOF modes are similar to those of Mestas-Nuñez and Enfield (1999). In those analyses, however, all months of the calendar year were used and the longer period (1856-1991) was included. The rotation procedure did not improve on the first unrotated mode's ability to represent Pacific variability associated with the PDO. However, the third unrotated mode, which best corresponds to the NAO in the North Atlantic, was found to include spatial features in other basins (eastern equatorial Pacific, South Atlantic) that split off into separate modes under rotation. Those REOFs correlate poorly (in time) with the only rotated mode that preserves the essence of the NAO variability in the North Atlantic: REOF-3. REOF-3 also explains almost as much variability as its unrotated parent (EOF-3): 3.4%. Hence, we will only discuss the first unrotated (EOF-1) mode and the third rotated mode (REOF-3) because they best help us to understand the canonical forms of the PDO and NAO, respectively.

Fig. 5 shows the spatial and temporal variability for the first, PDO-related EOF of the global SSTA residuals. As with the global ENSO mode (Fig. 2), the spatial pattern (top) is a map of gain (%) for the data with respect to the temporal reconstruction for the plotted rectangular region (bottom). Most of the dominant features of the PDO/SSTA composite (Fig. 3) are well reproduced in this mode for the Pacific basin. One is an area of strong anticorrelated variability that stretches across the central North Pacific along 30-50°N. Also seen is the strong in-phase variability along the Pacific eastern boundary, north and south of the equator. Another feature of the PDO/SSTA composite is the in-phase variability on and about the equator in the central and eastern tropical Pacific. Only the off-equatorial aspects of the PDO/SSTA composite (Fig. 3) are reproduced by EOF-1 (Fig. 5). The equatorial component was captured by EOF-2 (not shown; see Enfield and Mestas-Nuñez, 1999). The time variabilities in Figs. 3 and 5 correspond well and both contain the well-documented, recent phases of the PDO. Although the year-to-year (unsmoothed) variations in the PDO are less well correlated with EOF-1 (0.36) than are the decadal (smoothed) fluctuations (0.60), both correlations are about equally significant (95%) after accounting for serial correlation in the data.

Fig. 6 shows the rotated modal variability (REOF-3) corresponding to the NAO composite (Fig. 4). Because the region south of Greenland was chosen as the reference for the temporal reconstruction and the gain map, the signs of features in REOF-3 are opposite to those of the NAO in both the spatial and the temporal sense. Features in REOF-3 that are common with the NAO (but with opposite sign) are in-phase variability south of Greenland, in the tropical North Atlantic, and in a region off the west coast of North America. The reduced gain in the 20°N-40°N zonal band of the North Atlantic corresponds qualitatively to the reduced or opposite-sign composite values in the NAO distribution (Fig. 4). A feature from the NAO/SSTA composite that is not well reproduced by REOF-3 is the negative composite-mean region in the central equatorial Pacific. The temporal correlation between REOF-3 and the NAO is –0.35 (-0.41) for the unsmoothed (smoothed) series. After accounting for serial correlation, however, the association for the unsmoothed data is more significant (98%) than that of the smoothed data (90%).

Of special significance in REOF-3 (Fig. 6) is the fact that the varimax rotation did not separate the positive gains at the high latitudes of the North Pacific (especially the Gulf of Alaska) from the NAO-related features in the North Atlantic. This, combined with similar indications from the NAO composite mean distribution, suggests that SSTA at the high latitudes of both the Pacific and the Atlantic are tropospherically linked through fluctuations in the polar vortex. We can also see a spatial similarity in the North Pacific gain distributions of EOF-1 and REOF-3, especially in the region off the west coast of North America. The temporal reconstructions of EOF-1 and REOF-3 have a correlation of 0.59, suggesting that the two climate oscillations are linked through shared variability in that same west coast region and especially in the Gulf of Alaska.

Discussion: Implications for paleoclimates

Past climate variability at long timescales

There are many reasons to doubt that modern records can be used to make inferences about past background climates that lasted hundreds of years or more. The longest timescale in the instrumental record analyzed here is the secular trend, which might be representative of past variability at periods of 100-200 years, but probably not of millennial scales or longer. Moreover, given the similarity of the 20th century variations of the global mean SSTA (Fig. 1) to those of globally averaged air temperature (Houghton et al., 1996), it seems likely that a significant part of the trends and their spatial distribution may be anthropogenic and not necessarily representative of past natural variability, even for short intervals such as the LIA or MWP. It seems even less likely that any of the other climate modes presented here (ENSO, PDO, NAO) can serve as templates for how past climates of centennial or longer timescales differ from the modern climate. The physical processes that would produce significantly longer shifts would probably be quite different. This is especially true if interactive feedbacks are involved as we suspect is the case for the shorter timescales, since the timescales of oscillations such as ENSO are set by the nature of the processes involved. Specifically, the patterns of variability discussed here may not be representative of background climates in the early-to-mid Holocene or in Pleistocene glacial epochs.

The spatial similarities amongst the various modes analyzed here, especially in the Pacific, give us more optimism. The spatial self-similarity seen in the modes cuts across several timescales, despite the possibility that different processes are involved. Thus, even if we postulate that different timescales are governed by different subsurface ocean feedbacks (e.g., subduction at different locations or to different depths), many of the timescales and mechanisms may involve common elements that affect SSTA, such as the strength of the westerly wind belts. Moreover, the westerly wind strength will, in turn, affect the gyre circulations and their associated SST advection in similar ways. Finally, there remains the possibility, still unclarified by research, that interactive feedbacks are not crucial to long climate modes and that they merely arise from tha chaotic nature of atmospheric variability with the oceans responding passively (Sarachik et al., 1996).

Present climate modes and their associated SSTA patterns are, in fact, related to fluctuations in the strength of the westerly wind belts overlying major extratropical oceans, to the strength of the polar vortex and to changes in atmospheric pressure nodes surrounding the vortex. It is not difficult to surmise that the greater land and ice coverage that accompanied lower sea level stands would affect the same atmospheric features and on very long timescales. This is only speculation, however. Our best hope for understanding what those patterns may have been like must depend more on a combination of paleoclimatic proxy indicators and numerical modeling than on the analogies provided by modern climate scenarios. It is especially important that atmospheric models be forced with realistic surface boundary characteristics (sea level stand, ice cover and SST) as indicated by proxy data.

Just as in the 20th century, earlier background climates must have been accompanied by a full spectrum of variability on shorter timescales ranging down to the interdecadal and interannual periodicities described in this chapter. How similar that variability would be to the present variability is also best addressed by modeling. Whether or not a forced atmospheric model can accurately portray that variability depends on the ocean's role in producing and enhancing phase changes (Sarachik et al., 1996). If the ocean is an active and critical participant, coupled ocean-atmosphere models will be required. Present coupled models are precluded from doing this because of limitations having to do with resolution, integration time and stability. Until the models improve and debates about ocean interactivity are settled, paleoclimatologists should probably focus on improving the accuracy of the surface boundary conditions for past climates, especially as regards their SST distributions.

Holocene ENSO variability

A critical question, both for the modeling of current and future ENSO variability as well as past variability, is whether or not the characteristics of ENSO vary with the slowly evolving background climate. Our analysis of the global ENSO mode reveals more than a century of variability during which global warming has occurred (Fig. 1). However, we see no apparent differences in the return intervals and intensities of ENSO between one century and the next, at least not in the global ENSO mode derived from band-passed data (Fig. 2, bottom). Enfield and Cid (1991) were similarly unable to detect differences in El Niño return intervals between the Little Ice Age (LIA) and the 20th century. It is possible, however, that slowly varying, non-canonical aspects of recent ENSO events have been absorbed by the non-ENSO modes of variability. Whichever the case, we are left wondering if differences in background climate over much longer (multi-millennial) timescales are perhaps strong enough to trigger changes in ENSO behavior. This underscores the importance of determining how ENSO interacts with the interdecadal timescale fluctuations and how the longer timescale climate variability has varied in the past.

There is evidence, both from paleoclimate studies and from modeling, that ENSO variability has not been ubiquitous throughout the Holocene. Sandweiss et al. (1996) and previously Rollins et al. (1986) argue from the speciation record of molluscan assemblages along the north-central Peru coast that El Niño events started to occur about 5000 yr BP but were absent from the earlier to mid-Holocene (5000-8000 yr BP). Although the significance of the molluscan data has been debated and the conclusions contested (DeVries and Wells, 1990; DeVries et al., 1997; Wells and Noller, 1997; Sandweiss et al., 1997), there is independent evidence from lacustrine laminations in southwestern Ecuador to support the Sandweiss interpretation (Rodbell et al., 1999).

While the paleogeographic evidence is being sifted and debated, it is nevertheless of interest for climatologists to consider such a climate scenario. It has been recently argued on physical grounds that ENSO variability is required for the aperiodic removal (to polar regions) of excess heat that accumulates in the equatorial Pacific Ocean (Sun and Trenberth, 1998). If this is correct, then it may be that the background climates of prior epochs (e.g., the mid-to-early Holocene) had smaller pole-to-equator temperature contrasts and no need for the augmented poleward heat transport that is presently accomplished through El Niño events. One can speculate that such a climate would have lacked the equatorial Pacific characteristics that presumably lead to ENSO cycles at present, such as intensified trade winds, western Pacific accumulations of warm upper layer water, large zonal SST gradients, and an exaggerated eastward uptilt of the thermocline. Using a relatively simple model, Sun (1999, chapter ZZZ) illustrates how ENSO variability may be sensitive to the temperature contrast between the eastern and western Pacific, and the related availability (through thermocline uptilt) of cold-temperature thermocline water that can be upwelled and mixed into the surface layer in the eastern Pacific. Without the SST gradients that we see in non-El Niño years today, ENSO instabilities would not have arisen, ultimately because they would not have been required for the poleward removal of heat. The equatorial cold tongue would have been less well developed and the coastal temperatures off Peru would have been warmer (though still relatively cool and characterized by coastal upwelling), and without the alternation between warm and cold years (ENSO).

The above scenario, though speculative, is consistent with Sandweiss et al. (1996) and Rodbell et al. (1999) and also with other, independent findings. Thus, for example, there is evidence that the contrast in seasonal insolation between the equator and high latitudes has increased between the early and late Holocene (Berger, 1978), consistent with smaller meridional temperature differences before 5000 BP and a lack of ENSO activity. Consistent with a (previously) warmer Peru coastal climate, there is ice core evidence that the climate of the adjacent north-central Peru highlands was warmer during the 5000-8000 yr BP period in question (Thompson et al., 1995).

What aspect of the background climate might account for a warmer thermocline temperature? A possible clue lies in the self-similarity in SSTA patterns across timescales. In three separate SSTA patterns — secular (Fig. 1), ENSO (Fig. 2) and interdecadal (Fig. 5) — we see common elements that differ mainly in their intensities. One is a general warmth (coolness) in the low latitudes of the eastern Pacific extending poleward off the coasts of North and South America, and as far as the Gulf of Alaska in the north. Also seen in all threes is an area of cool (warm) temperatures across the mid-latitudes of the central North Pacific. The latter feature, in particular, is important because it extends across the subtropical convergence zone north of Hawaii, a region of ocean instability where the mixing of upper ocean water by winter storms can entrain surface water to thermocline depths. This water is of an appropriate density to be transported by a circuitous route along the thermocline to low latitudes where it can upwell on or near the equator (Gu and Philander, 1997). An oscillation presumably occurs because as thermocline water becomes warmer and/or deeper at low latitudes, cooler water is entrained at the high latitudes to replace it, reversing the cycle. Because the transit from the central North Pacific to the equator requires the better part of a decade, the timescale associated with maximum amplitude across the subtropical convergence is the interdecadal.

There is a problem in applying this self-similar pattern to the millennial timescale, however. To produce a quasi-stationary (very long timescale) change in the background temperature of the tropical thermocline, the mid-latitude thermal anomaly across the subtropical convergence would have to be of the same sign. That, or some entirely different reversal mechanism with a much longer oscillation timescale would have to be involved, because water mass trajectories at tropical thermocline depths do not have millennial (or even centennial) transit times.

This discussion has identified several areas where further paleoclimate research can be especially fruitful. Although we can see some enticing areas of convergence between paleoclimate scenarios for Holocene changes in ENSO variability, and inferences from the instrumental climate record (Figs. 1, 4), inconsistencies remain. Further paleoclimatic evidence is needed to determine whether a background ocean climate consistent with current theories existed (e.g., Sun, 1998) and whether the Peru coastal climate was consistent with a warmer but steady east Pacific (e.g., with increased coastal rainfall). In regard to the former, studies such as CLIMAP should consider variations, vis-à-vis the present, in the pole-to equator SST differences and in the subtropical subduction regions of the North and South Pacific. In regard to the latter, paleogeographers have yet to uncover evidence of the increased vegetation that would be expected of a warmer (albeit semi-arid) coastal climate. It must also be hoped that paleoecologists can clarify what kind of an ocean climate (steady, but how much warmer?) would support the observed warm-water molluscan assemblages during the 5000-8000 yr BP period, and discourage the cold-water species observed after 5000 yr BP. Finally, inconsistencies in the paleomarkers of the early-to-mid Holocene climate of Peru, such as noted by DeVries and Wells (1990), must be addressed.

Acknowledgments. J. Harris prepared all of the basic data sets used in this project. We are grateful to one of the reviewers (M. Dettinger) for his extraordinary thoroughness and his many helpful comments. This work has been supported by base funding from the Environmental Research Laboratories, by a grant from the Pan-American Climate Studies program, and by a grant from the Inter-American Institute for Global Change Research (IAI).

References

Barnston, A. G. and R. E. Livezey, 1987: Classification, seasonality and persistence of low-frequency atmospheric circulation patterns. *Monthly Weather Review*, 115: 1083-1126.

Berger, A., 1978: Long-term variations of caloric insolation resulting from the Earth's orbital elements. *Quaternary Research*, 9: 139-167.

Bjerknes, J., 1964: Atlantic Air-sea interaction. *Avances in Geophysics*, 10, Academic Press, 1-82.

Curry, R.G., M.S. McCartney, and T.M. Joyce, 1998: Oceanic transport of subpolar climate signals to mid-depth subtropical waters. *Nature*, 391: 575-577.

D'Arrigo, R.D., E.R. Cook, and G.C. Jacoby, 1996: Annual to decadal-scale variations in northwest Atlantic sector temperatures inferred from tree rings. *Canadian Journal of Forrest Research*, 26: 143-148.

Dettinger, M.D., D.S. Battisti, G.M. McCabe, Jr., and R.D. Garreaud, 1999: Interhemispheric effects of interannual and decadal ENSO-like climatic variations in the Americas. In: *Present and Past Inter-Hemispheric Climate Linkages in the Americas and their Societal Effects*, V. Markgraf, ed., Cambridge University Press, Cambridge.

DeVries, T.J., L. Ortlieb, A. Diaz, L. Wells, and Cl. Hillaire-Marcel, 1997: Determining the early history of El Niño. *Science*, 276: 965-966.

DeVries, T.J., and L.E. Wells, 1990: Thermally-anomalous Holocene molluscan assemblages from coastal Peru: evidence for paleogeographic, not climatic change. *Palaeogeography, Palaeoclimatology, Palaeoecology*, 81: 11-32.

Enfield, D.B., and L. Cid S., 1991: Low-frequency changes in El Niño-Southern Oscillation. *Journal of Climate*, 4: 1137-1146.

Enfield, D.B. and D.A. Mayer, 1997: Tropical Atlantic SST variability and its relation to El Niño-Southern Oscillation. *Journal of Geophysical Research*, 102: 929-945.

Enfield, D.B. and A.M. Mestas-Nuñez, 1999: Multiscale variabilities in global sea surface temperatures and their relationships with tropospheric climate patterns. *Journal of Climate* (in press).

<Evans et al., 1999: authors & title pending>. In: *Present and Past Inter-Hemispheric Climate Linkages in the Americas and their Societal Effects*, V. Markgraf, ed., Cambridge University Press, Cambridge.

Gray, W. M., 1990: Strong association between West African rainfall and US landfall of intense hurricanes. *Science,* 249: 1251-1256.

Gu, D., and S.G.H. Philander, 1997: Interdecadal climate fluctuations that depend on exchanges between the tropics and extratropics. *Science,* 275: 721-892.

Hastenrath, S., L.C. de Castro, and P. Aceituno, 1987: The Southern Oscillation in the Atlantic sector. *Contributions in Atmospheric Physics,* 60: 447-463.

Houghton, J.T., L.G. Mehra Filho, B.A. Callander, N. Harris, A. Kattenberg and K. Maskell, eds., 1996. *Climate Change 1995, the Science of Climate Change: Contribution of WGI to the Second Assessment Report of the Intergovernmental Panel on Climate Change,* Cambridge Univ. Press, Cambridge, 1996.

Hunt, B.G., 1998: Natural climatic variability as an explanation for historical climate fluctuations. *Climatic Change*, 38: 133-157.

Hurrell, J.W., 1995: Decadal trends in the North Atlantic Oscillation, regional temperatures and precipitation. *Science,* 269: 676-679.

Kaplan, A., M.A. Cane, Y. Kushnir, A.C. Clement, M.B. Blumenthal, and B. Rajagopalan, 1998: Analyses of Global Sea Surface Temperature 1856-1991. *Journal of Geophysical Research*, 103: 18,567-18,589.

Landsea, C.W., R.A. Pielke, A.M. Mestas-Nuñez, and J.A. Knaff, 1999: Atlantic basin hurricanes: Indices of climatic changes. *Climatic Change.* (in press)

Lanzante, J. L., 1996: Lag relationships involving tropical sea surface temperatures. *Journal Physical Oceanography,* 9: 2568-2578.

Latif, M., and T. P. Barnett, 1994: Causes of decadal climate variability over the North Pacific and North America. *Science,* 266: 634-637.

Latif, M., and T. P. Barnett, 1995: Interactions of the tropical oceans. *Journal of Climate,* 8: 952-964.

Latif, M., and T. P. Barnett, 1996: Decadal climate variability over the North Pacific and North America: dynamics and predictability. *Journal of Climate,* 9: 2407-2423.

Lau, N.-C., and M.J. Nath, 1994: A modeling study of the relative roles of tropical and extratropical anomalies in the variability of the global atmosphere-ocean system. *Journal of Climate,* 7: 1184-1207.

Mantua, N., S.R. Hare, Y. Zhang, J.M. Wallace, and R.C. Francis, 1997: A Pacific interdecadal climate oscillation with impacts on salmon production. *Bulletin of the American Meteorological Society,* 78: 1069-1079.

Mestas-Nuñez, A.M. and D.B. Enfield, 1999: Rotated global modes of non-ENSO sea surface temperature variability. *Journal of Climate* (in press).

Muck, P., 1989: Major trends in the pelagic ecosystem off Peru and their implications for management, p. 386-403. *In:* D. Pauly, P. Muck, J. Mendo and I. Tsukuyama (eds.), *The Peruvian Upwelling System: Dynamics and Interactions.* ICLARM Conference Proceedings, 18, 438 p. Instituto del Mar del Peru (IMARPE), Callao, Peru; Deutsche Gesellschaft für Technische Zusammenarbeit (GTZ) GmbH, Eschbom, Federal Republic of Germany; and International Center for Living Aquatic Resources (ICLARM), Manila, Philipines.

Nakamura, H., G. Lin, and T. Yamagata, 1997: Decadal climate variability in the North Pacific during the recent decades. *Bulletin of the American Meteorological Society*, 78: 2215-2225.

Nicholson, S. E., 1989: Long-term changes in African rainfall. *Weather*, 44: 46-56.

Quinn, W.H., V.T. Neal and S. Antunez de Mayolo, 1987: El Niño occurrences over the past four and a half centuries. *Journal of Geophysical Research,* 92: 14,449-14,461.

Rodbell, D., G.O. Seltzer, D.M. Anderson, D.B. Enfield, M.B. Abbott, J.H. Newman, 1999: A high-resolution ~15,000 year record of El Niño driven alluviation in southwestern Ecuador. *Science*, 283, 516-520.

Rollins, H.B., J.B. Richardson, and D.H. Sandweiss, 1986: The birth of El Niño: Geoarchaeological evidence and implications. *Geoarchaeology*, 1: 3-15.

Sandweiss, D.H., J.B. Richardson III, E.J. Reitz, H.B. Rollins, and K.A. Maasch, 1996: Geoarchaeological evidence from Peru for a 5000 years B.P. onset of El Niño. *Science*, 273: 1531-1533.

Sandweiss, D.H., J.B. Richardson III, E.J. Reitz, H.B. Rollins, and K.A. Maasch, 1997: Determining the early history of El Niño. *Science*, 276: 966-967.

Sarachik, E.S., M. Winton, and F.L. Yin, 1996: Mechanisms for decadal-to-centennial climate variability. *In* D.L.T. Anderson and J. Willebrand (eds.), *Decadal Climate Variability.* NATO ASI Series I: Global and Environmental Change, Vol. 44. New York: Springer-Verlag, 157-210.

Smith, T.M., R.E. Livezey and S.S. Shen, 1998: An improved method for analyzing sparse and irregularly distributed SST data on a regular grid: The tropical Pacific Ocean. *Journal of Climate,* 11: 1717-1729.

Sun, D.-Z., 1998: Global climate and ENSO: A theoretical framework. In: *El Niño and the Southern Oscillation: MultiscaleVariability, Global and Regional Impacts on*

Natural Ecosystems and Society, H.F. Diaz and V. Markgraf, eds, Cambridge University Press (in press).

Sun, D.-Z., and K.E. Trenberth, 1998: Coordinated heat removal from the equatorial Pacific during the 1986-87 El Niño. *Geophysical Research Letters*, 25: 2659-2662.

Thompson, L.G., E. Mosley-Thompson, M.E. Davis, P.-N. Lin, K.A. Henderson, J. Cole, J.F. Bolzan, and K.-b. Liu, 1995: Late glacial stage and Holocene ice core records from Huascarán, Peru. *Science*, 269: 46-50.

Trenberth, K.E. and T.J. Hoar, 1996: The 1990-1995 El Niño-Southern Oscillation event: Longest on record, *Geophysical Research Letters*, 23: 57-60.

Trenberth, K.E. and J.W. Hurrell, 1994: Decadal atmosphere-ocean variations in the Pacific, *Climate Dynamics*, 9: 303-319.

Timmerman, A., M. Latif, R. Voss, and A. Grotzner, 1998: Northern Hemispheric interdecadal variability: A coupled air-sea mode. *Journal of Climate,* 11: 1906-1931.

Wells, L., and J.S. Noller, 1997: Determining the early history of El Niño. *Science*, 276: 966.

Wiles, G.C., R.D. D'Arrigo and G.C. Jacoby, 1998: Gulf of Alaska atmosphere-ocean variability over recent centuries inferred from coastal tree-ring records. *Climatic Change*, 38: 289-306.

Woodruff, S.D., R.J. Slutz, R.L. Jenne and P.M. Steurer, 1987: A comprehensive ocean-atmosphere data set. *Bulletin of the American Meteorological Society,* 68: 1239-1278.

Figure Captions:

Fig. 1. A: Distribution of the 1856-1991 linear (least-squares) trend (°C/century) in the smoothed Kaplan et al. (1998) SSTA data set. The contour interval is 0.2 °C/century, the heavy contour is zero, and the light solid (dashed) contours are positive (negative). Positive trends exceeding 0.2 °C/century are shaded. B: Time variation of the global average SSTA.

Fig. 2. First complex empirical orthogonal function (CEOF), describing the global El Niño-Southern Oscillation (ENSO) variability. A: Spatial distribution of the amplitude with respect to the modal reconstruction over the NINO3 index region (white rectangle, B). Contours shown are 10, 30, 60 and 90, and values in excess of 10 are shaded. A score of 100 is the average amplitude over the NINO3 region. B: Spatial distribution of phase lag (seasons); +/- indicates that the data lags/leads NINO3 (C) by one season and positive numbers indicate data lags of more than one season. C: Temporal reconstruction of the mode-related variability averaged over the NINO3 index region.

Fig. 3. Composite analysis of the Pacific Decadal Oscillation (PDO) for the December-January-February (DJF) season. A: The smoothed (dark) and unsmoothed (light) versions of a PDO temporal index defined by averaging sea level pressure anomaly (SLPA) over an area near the Aleutian Islands and 170°W, signed so as to represent the strength of the mid-latitude westerly winds in the North Pacific (see text for details). B: Distribution of the difference between the composite averages of SLPA over the Northern Hemisphere for positive and negative phases of the unsmoothed PDO index. Units are in hectoPascals (hPa). C: Distribution of the difference of composites of SSTA, similarly calculated for the phases of the PDO index. Units are in °C.

Fig. 4. As in Fig. 3, but for a DJF version of the North Atlantic Oscillation (NAO) index defined by Hurrell (1995).

Fig. 5. First empirical orthogonal function (EOF) of the non-ENSO residual data set, describing the Pacific interdecadal variability for the DJF season. A: Spatial distribution of the response with respect to the modal reconstruction over the index region (rectangle); contour interval is 40 and dashed contours are negative. Positive gain in excess of 40 is shaded. A score of 100 is the average response over the index region. B: Temporal reconstruction of the mode-related variability averaged over the index region.

Fig. 6. As in Fig. 3, but for the third rotated EOF (REOF) of the non-ENSO residual data set, describing the Atlantic multidecadal variability for the DJF season.

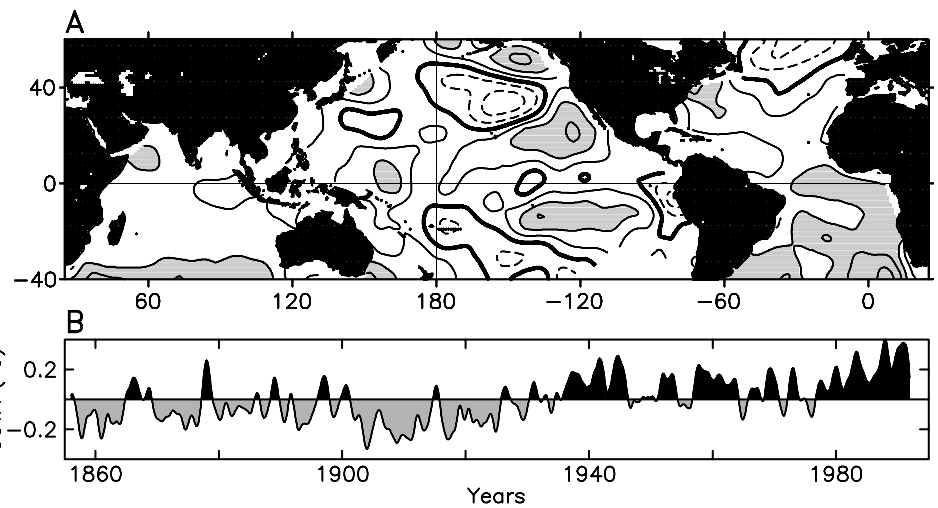
A
40
0
−40
60
120
180
−120
−60
0
B
SSTA (°C)
0.2
−0.2
1860
1900
1940
1980
Years

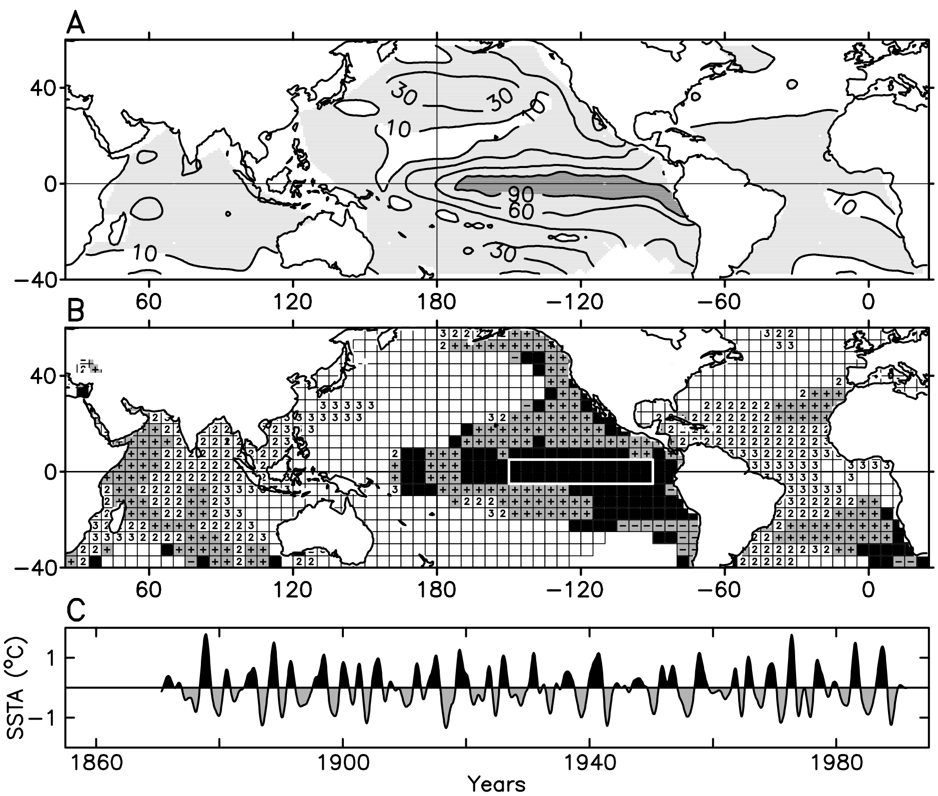
A
B
C
40
0
−40
60
120
180
−120
−60
0
SSTA (°C)
1
−1
1860
1900
1940
1980
Years

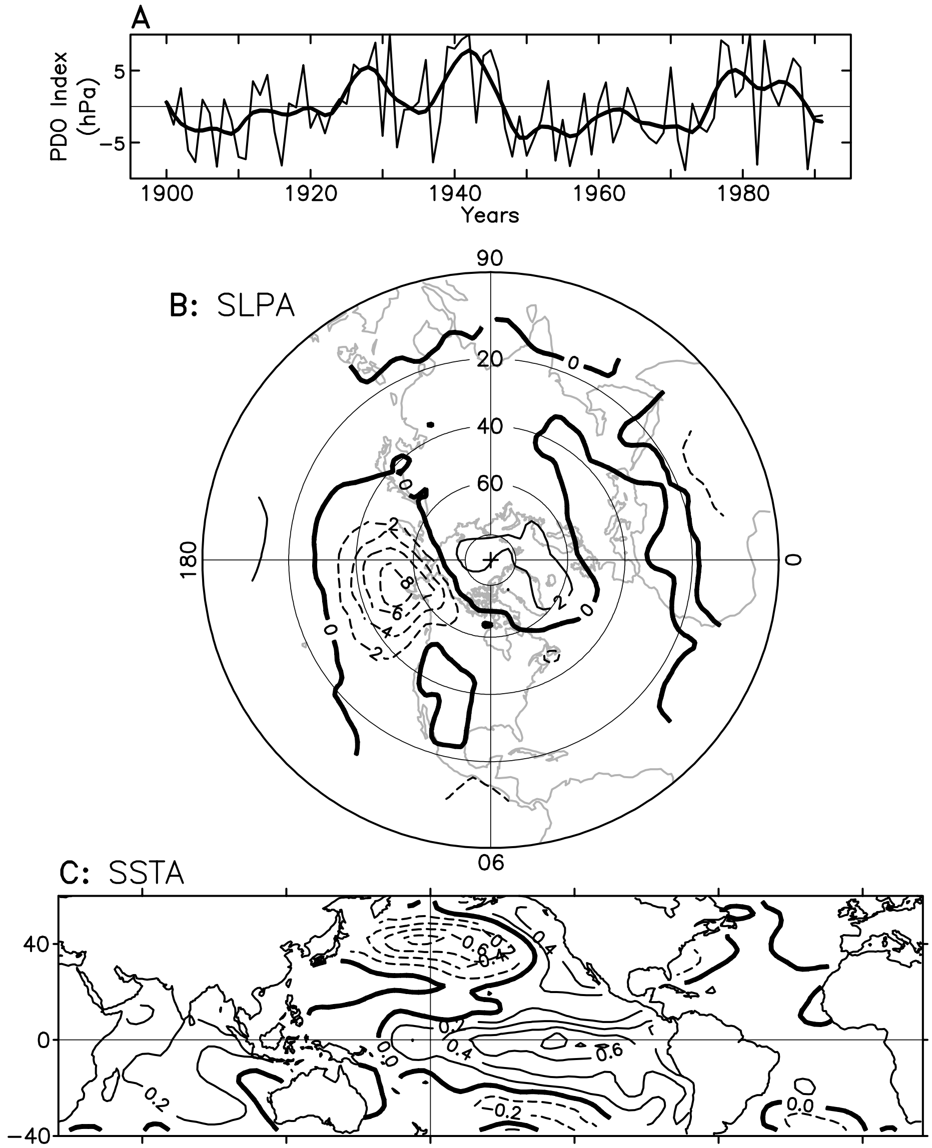

A
PDO Index
(hPa)
5
−5
1900
1920
1940
1960
1980
Years
B: SLPA
90
20
40
60
180
0
06
C: SSTA
40
0
−40
60
120
180
−120
−60
0

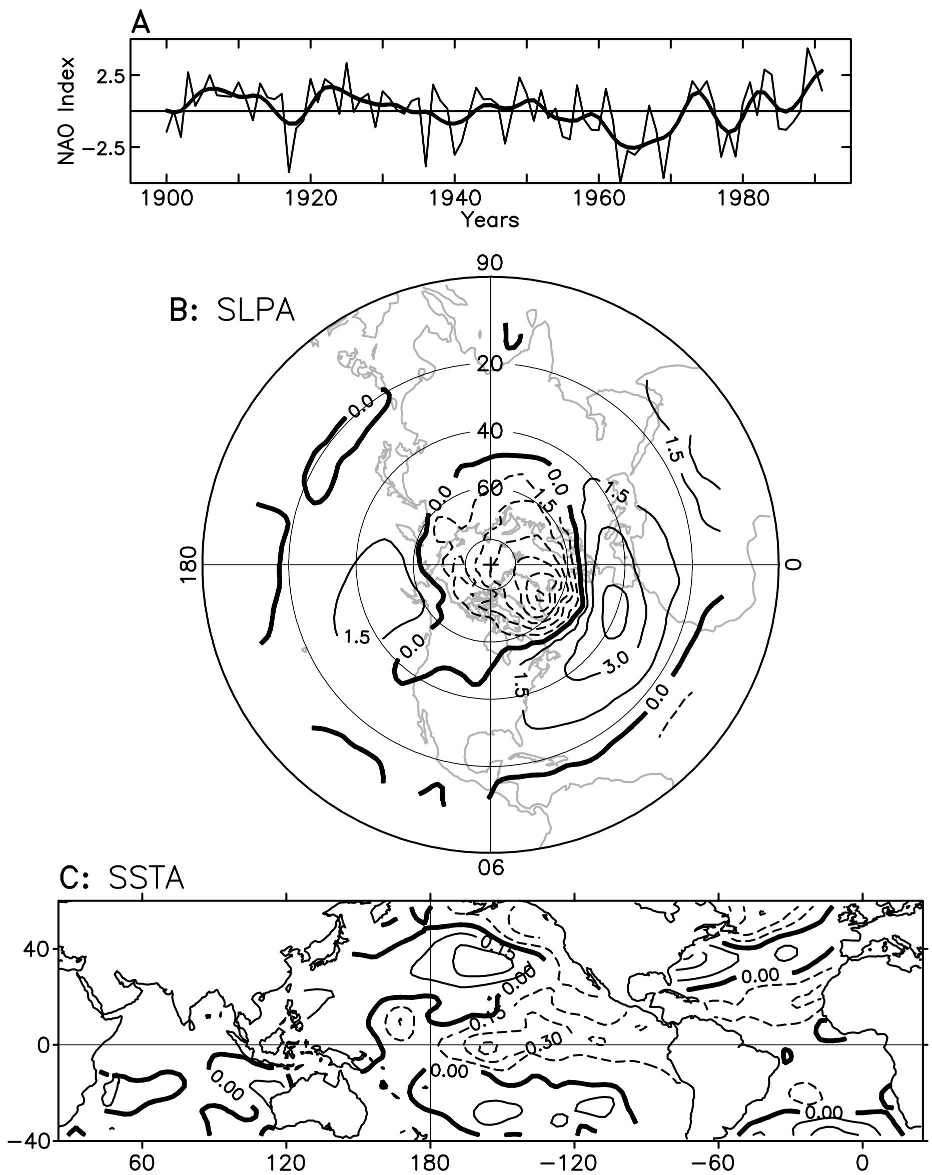

A
NAO Index
2.5
−2.5
1900
1920
1940
1960
1980
Years
B: SLPA
90
180
0
06
20
40
60
0.0
1.5
3.0
C: SSTA
40
0
−40
60
120
180
−120
−60
0
0.00
0.15
0.30

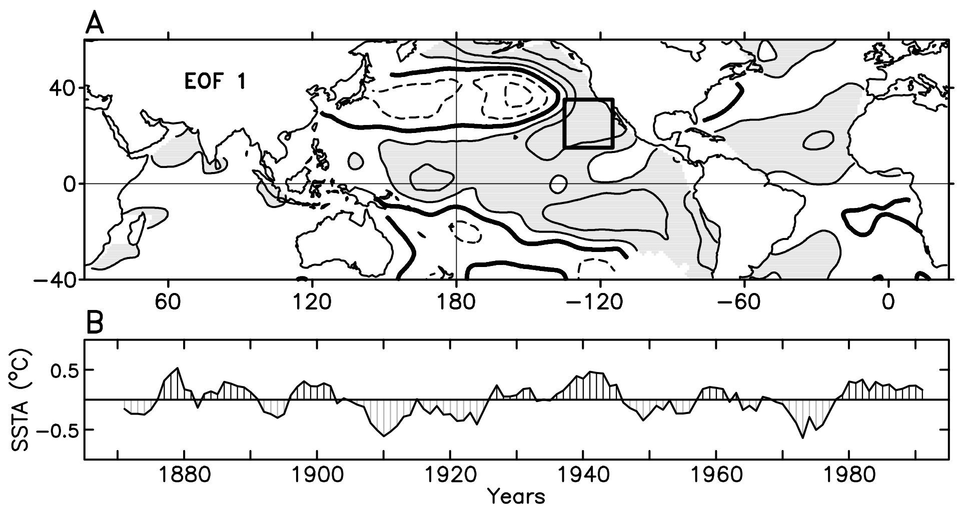
A
EOF 1
40
0
−40
60
120
180
−120
−60
0
B
SSTA (°C)
0.5
−0.5
1880
1900
1920
1940
1960
1980
Years

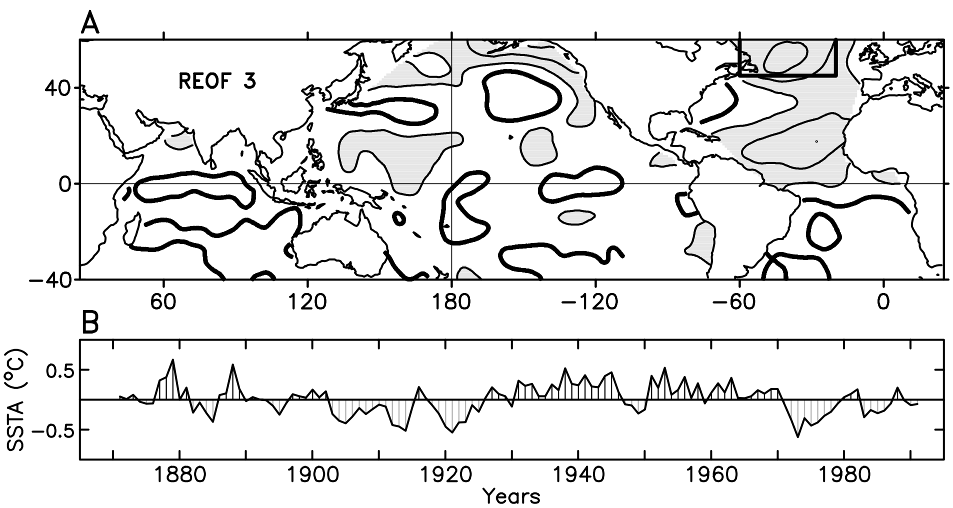
A
REOF 3
40
0
−40
60
120
180
−120
−60
0
B
SSTA (°C)
0.5
−0.5
1880
1900
1920
1940
1960
1980
Years